Nuclear shape transitions, level density, and underlying interactions

S. Karampagia and Vladimir Zelevinsky

Phys. Rev. C **94**, 014321 — Published 28 July 2016

DOI: 10.1103/PhysRevC.94.014321

Nuclear shape transitions, level density, and underlying interactions

S. Karampagia and Vladimir Zelevinsky

National Superconducting Cyclotron Laboratory and Department of Physics and Astronomy, Michigan State University, East Lansing, MI 48824-1321, USA

Abstract

Background: The configuration interaction approach to nuclear structure uses the effective Hamiltonian in a finite orbital space. The various parts of this Hamiltonian and their interplay are responsible for specific features of physics including the shape of the mean field and level density. This interrelation is not sufficiently understood.

Purpose: We intend to study phase transitions between spherical and deformed shapes driven by different parts of the nuclear Hamiltonian and to establish the presence of the collective enhancement of the nuclear level density by varying the shell-model matrix elements.

Method: Varying the interaction matrix elements we define, for nuclei in the sd and pf shells, the sectors with spherical and deformed shapes. Using the moments method that does not require the full diagonalization we relate the shape transitions with the corresponding level density.

Results: Enhancement of the level density in the low-energy part of the spectrum is observed in clear correlation with a deformation phase transition induced mainly by the matrix elements of single-particle transfer.

Conclusions: The single-particle transfer matrix elements in the shell model nuclear Hamiltonian are indeed the carriers of deformation, providing rotational observables and enhanced level densities.

PACS numbers: 21.60.Cs, 21.10.Ma, 05.30.Rt

I. INTRODUCTION

The knowledge of the level density in a quantum many-body system is necessary for the correct understanding of the response of the system to external perturbations. The nuclear level density is a vitally important element of reaction theory, including astrophysical processes and broad applications of nuclear physics. But it might also serve as a mirror reflecting special features of intrinsic structure and this will be the main subject of our consideration.

In a Fermi-system environment, the level density exponentially grows with energy due to the combinatorics of particle-hole excitations from the defrosted Fermi surface. This occurs even in the simplest picture of a Fermi gas without residual interaction [1, 2]. The Fermi gas model does not however account for the effects on the level density due to the shell structure, pairing correlations [3, 4] or coherent excitations of collective nature [5, 6]. Various semi-phenomenological approaches have been developed which account for such effects [7, 8] considered as additions to the skeleton of the Fermi-gas, or of a more elaborate self-consistent mean field with pairing.

Low-lying collective modes, mainly of isoscalar nature, lead to the reconfiguration of the nuclear spectra. In an even-even non-magic nucleus, pairing correlations create an energy gap in the excitation spectrum. Inside the gap vibrational collective modes start the sequence of phonon states which gradually mix with unpaired particles appearing above the pair breaking threshold. Away from the magic nuclei, the accumulating valence particle frequently lead to broken internal symmetry and static deformation of the core. Then nuclear rotation appears as a new branch of the excitation spectrum. The rotational bands, with a small distortion of the nuclear field along the band, appear at low energy. All these effects should noticeably change the low-lying nuclear level density [9–11].

In the framework of the shell model, pairing and collective effects are fully taken into account through the two-body interaction matrix elements. Since the shell model is formulated in a truncated orbital space and therefore has the fixed total number of quantum states, the collective enhancement can appear as enrichment of the level density at the low-energy part of the spectrum, accompanied by a corresponding suppression of the level density at higher excitation energy. The shell-model experience shows that the effects of deformation and related rotational motion appear naturally for a sufficiently rich space and appropriate

set of two-body interaction matrix elements as a result of the diagonalization in a spherical basis. This is an important advantage of the shell-model approach since one does not need to take special care of the strict fulfillment of conservation laws (particle number, angular momentum, parity and isospin). On the other hand, the computational problems impose the limitation on the total dimension of the orbital space.

The *moments method* based on statistical properties of large Hamiltonian matrices [12, 13] was recently formulated [14, 15] as a practical tool for calculating the level density for a given Hamiltonian avoiding the diagonalization of large matrices. It was shown how the first two moments of the Hamiltonian define the full level density that coincides with the result of the exact diagonalization if the latter is feasible. Some latest results and first comparisons with the phenomenology, thermodynamics, and mean field combinatorics can be found in [16]. One important conclusion is that in realistic cases the level density in a finite Hilbert space is a smooth bell-shape curve. The contributions of individual shells, which are clearly pronounced in the mean-field combinatorics, are smeared by the multitude of incoherent collision-like interactions which are always present in realistic Hamiltonians in addition to the collective parts like pairing and multipole forces. In this article, our problem is rather different. We are going to explore the landscape of nuclear Hamiltonians varying the parameters in order to establish the existence and dynamic sources of the collective enhancement of the level density. We use the moments method to extract the cases with collective behavior and study the corresponding level densities. This method was used earlier [17] for understanding the predominance of prolate deformation among non-spherical nuclei. With the variation of parameters of the shell-model Hamitonian, we are able to localize and study the phase transitions between spherical and deformed shapes.

In Section 2 we give a brief description of the moments method, in Section 3 we describe the division of the full shell-model Hamiltonian into different subsets of matrix elements which can be varied independently. Section 4 presents the effects of those subsets on the low-lying spectrum of different nuclear systems and on the level densities. In Section 5 we discuss a quantum phase transition between spherical and deformed shapes by varying the strength of the matrix elements. The concluding discussion is given in Section 6.

II. MOMENTS METHOD

Here we very briefly remind the formalism of the moments method. We use the shell-model Hamiltonian H that contains the mean field and residual two-body effective interactions. The level density is found as a superposition of modified (finite range) Gaussians,

$$\rho(E;\alpha) = \sum_p D_{\alpha p} G_{\alpha p}(E). \tag{1}$$

Here α stands for the exact quantum numbers of spin and parity, while p runs over partitions (distributions of particles among available single-particle orbitals); $D_{\alpha p}$ is the dimension of a given partition, and $G_{\alpha p}$ is the finite-range Gaussian determined by the ground state energy, the centroid (the first moment of the Hamiltonian) and the width (the second moment). The second moment includes all interactions mixing the partitions. Both moments can be computed directly by the Hamiltonian matrix avoiding its diagonalization. As we have already mentioned, the result (1) is, in all studied cases, in good agreement with the product of the full diagonalization if the latter is practically possible.

Technical details related to finding the ground state energy, M-scheme against J-scheme, fit of the spin cut-off parameter, removal of unphysical center-of-mass excitations in the cases of cross-shell transitions etc. are discussed in previous publications [14–16].

III. SEARCHING FOR COLLECTIVE EFFECTS

In the simplest (but still rich in physics and numerous applications) case of the *sd* shell model we have only three single-particle levels, $1s_{1/2}, 0d_{5/2}, 0d_{3/2}$. The angular momentum and isospin conservation allow 63 matrix elements of the residual two-body interactions. Keeping intact all symmetry requirements, we can vary numerical values of the two-body matrix elements of the effective interaction. As a result, we come to different versions of the shell model which can cover the whole spectral variety allowed by the given Hilbert space. In this way we can select the parts of the interaction responsible for specific observable physical phenomena.

In a recent study [17], where in the same spirit the pf orbital space was used, it was found that certain interaction matrix elements are responsible for the transition from a spherical shape to a deformed one. First of all, they were the matrix elements (pf matrix elements in

that specific model) changing the occupation numbers of the subshells by one unit, i.e. the matrix elements $\langle j_k, j_l|V|j_m, j_n\rangle$ with $j_k = j_m$, or $j_k = j_n$, or $j_l = j_m$, or $j_l = j_n$. This drives the mixing of spherical orbitals in the process of deformation. A complementary version of a similar approach was applied in [16] in order to demonstrate that the incoherent parts of the residual interaction are essential for producing chaotic wave functions and resulting smooth level density.

Borrowing this approach we divide the set of interaction matrix elements into two parts. The part V_1 includes the "particle-hole" matrix elements which change the occupation number of the subshells by one unit with the change of orbital momentum $\Delta\ell = 0\,\text{or}\,2$, whereas the part V_2 includes the remaining matrix elements, which either don't change the occupation number of the subshells ($j_k = j_m$ and $j_l = j_n$), or change it by two units ($j_k \neq j_m$ and $j_k \neq j_n$),

$$H = h + k_1 V_1 + k_2 V_2; \tag{2}$$

here the part h contains the single-particle energies. From this point on we will be calling the matrix elements of the V_1 part, "one unit change" matrix elements. The numerical parameters k_1 and k_2 allow us to explore regions of the Hilbert space where the nuclear structure undergoes significant changes. The original shell-model case emerges for $k_1 = k_2 = 1$. Probing various combinations of parameters k_1 and k_2 one can see how these two parts affect the level density and other observable quantities of interest. We will study the evolution of the level density as a function of these particular interaction modes paying special attention to the low-lying parts of the spectrum as indicators of characteristic underlying structures. In even-even nuclei we characterize the low-lying spectrum by the levels (2^+, 4^+, 6^+), quadrupole transitions between them, and shape multipoles, as well as by the resulting level density.

IV. EXPLORING THE NUCLEAR LANDSCAPE

This section presents a quantitative study of how the V_1 and V_2 parts of the shell-model Hamiltonian (2) change the collective observables. We find whether these interactions are capable of producing typical deformed or spherical characteristics of the nuclear field in the low-energy part of the nuclear spectrum.

Two shell model spaces, the sd and pf, have been studied. As already mentioned, the

interaction of the *sd* shell-model space has 63 non-zero matrix elements, among which 22 elements induce one-body transitions between the partitions (these are included in the V_1 part of eq. (2), while the remaining 41 matrix elements (those included in the part V_2 of eq. (2) either couple states within the same partition or transfer two particles between partitions, including usual pairing.

In the same spirit, the interaction in the pf shell has 195 non-zero matrix elements, 79 of which are included in the V_1 part of eq. (2), while 116 remaining matrix elements, which either don't change the occupation number of the subshells or induce two-body transitions between the partitions, make up the V_2 part of eq. (2). We have considered the cases with four valence protons + four valence neutrons and six valence protons + six valence neutrons for the *sd* shell (these correspond to the ^{24}Mg and ^{28}Si nuclei, respectively) and the case of six valence protons + six valence neutrons for the pf shell model (the ^{52}Fe nucleus).

The observables used for studying the effects of various parts of the interaction are the low-lying 2_1^+ and 4_1^+ energy levels, the ratio of these energies, $R_{4/2}$=$E(4_1^+)/E(2_1^+)$, the expectation value of the quadrupole moment in the first excited state, $Q(2_1^+)$ and the reduced quadrupole transition probability, $B(\mathrm{E2};2_1^+ \rightarrow 0_1^+)$. In order to distinguish between spherical and deformed cases, we use as an indicator the ratio $R_{4/2}$, which should be close to 2 for spherical shapes and close to 3.3 for deformed shapes. Selected results of the exact shell-model analysis are shown in Tables I and II.

Tables I-II display a pattern of correspondence between the tabulated nuclear observables and the evolution of one of the Hamiltonian parameters, either k_1 or k_2, while the other one is kept constant. In the first case, when $k_1 = 1$ is constant whereas k_2 evolves, the behavior of the ratio $R_{4/2}$ is very similar for the cases of ^{24}Mg and ^{52}Fe: this ratio first increases reaching a maximum above 3 around $k_2 = 0.5$ and then decreases for larger values of k_2. The behavior is slightly different for ^{28}Si having first a minimum at $k_2 = 0.2$ but evolving after that in the same way as in the two previous cases. The absolute energies of the 2_1^+ and 4_1^+ states increase slowly up to the maximum point of $R_{4/2}$, while after that the increase of the 2_1^+ and 4_1^+ energies is more pronounced. For the majority of the k_2 values, the ratio $R_{4/2}$ is closer to the rotational limit. The reduced transition probabilities $B(\mathrm{E2};2_1^+ \rightarrow 0_1^+)$ are quite strong for different values of k_2 of the first case, their values being close to or over 100 $\mathrm{e}^2 \cdot \mathrm{fm}^2$. As expected, the "one unit change" matrix elements are to a large extent responsible for the rotational characteristics, but they still need certain cooperation of other

matrix elements to create typical characteristics of deformation, while a too large value of other matrix elements destroys the rotational features. The discontinuity observed for ^{28}Si at small values of k_2 is accompanied by a sudden change of the quadrupole moment.

The effects of the V_2 part of the interaction with respect to various observables can be studied using Table II, where the parameter k_2 is fixed at the realistic level of 1.0 while k_1 evolves. The dynamics generated by only the two-body matrix elements which don't change the occupation number of the subshells or induce two-body transitions between the partitions is not capable of creating noticeable characteristics of deformation. The increase of k_1 drives a regular decrease of the 2_1^+ level and a steady growth of the $R_{4/2}$ ratio, a sign that the deformation trend is under way, though without ever reaching a pure rotational pattern. A steady increase is also observed for the $B(\mathrm{E2};2_1^+ \rightarrow 0_1^+)$ reduced transition probabilities, whose values are however lower than 100 $\mathrm{e}^2 \cdot \mathrm{fm}^2$ in the majority of cases, except for ^{52}Fe, whose transition rates $B(\mathrm{E2};2_1^+ \rightarrow 0_1^+)$ are still less strong compared to the corresponding cases with $k_1 = 1.0$ and k_2 evolving.

It is expected that the occurrence of rotational motion will increase the low-lying level density relative to spherical nuclei because of the contribution of emerging rotational bands. Among the different cases of Tables I and II we selected those that display values of $R_{4/2}$ and A close to rotational and spherical limits. As can be seen in Table III, the cases with rotational values present an enhancement of the level density of the $J = 0$ states in the lowest part of the energy spectrum compared to their spherical counterparts. These results are almost independent of angular momentum and apply even for low energies (i.e. the calculation of level density up to 3 MeV would give qualitatively the same results). The cumulative number of levels (NoL) was calculated using the moments method. It is convenient for comparison to renormalize the level density of the moments method making all level densities centered at 1. The normalization is achieved by dividing the width of the bin of the original Gaussian distribution, which is one, by the mean of the Gaussian found using $\frac{N_1 * x_1 + N_2 * x_2 + \ldots}{N_1 + N_2 + \ldots}$, where N_i is the number of levels in the energy bin, and x_i is the mean of the energy bin. In this way all Gaussians get centered at 1.

This part of the study clarifies the role of the "one unit change" matrix elements. The strong presence of the V_1 part of the shell-model interaction (responsible for mixing of orbitals of the same parity) is associated with deformational characteristics of the low-lying part of the spectrum. The strong presence of the V_2 part of the interaction drives the values

of all observables away from the rotational limit. This situation extends also to the level densities. Not only all rotational cases have a larger number of low-energy levels compared to their spherical counterparts, but also they are all observed for $k_1 = 1.0$, while all spherical cases are observed for $k_2 = 1.0$.

V. SIGNATURES OF A QUANTUM PHASE TRANSITION

In the previous section we studied the behavior of the two different parts of the Hamiltonian, by keeping one part constant and dominant and changing the other. In this way we saw that the dominant part gave either rotational ($k_1 = 1.0$) or spherical ($k_2 = 1.0$) characteristics to the spectrum. In this section we concentrate on a quantum phase transition that takes place when we change simultaneously the strength of the two parts of the Hamiltonian.

Nuclear models have long provided a fertile ground for studying phase transitions in mesoscopic quantum systems. Quantum phase transitions [18–23] occur when the special observables of a system, called order parameters, reveal structural, often geometrical, changes as a function of control quantities. It is convenient to study a quantum phase transition using a Hamiltonian of the form

$$H = h + (1 - \lambda)V_1 + \lambda V_2, \tag{3}$$

where the single particle energies part h is fixed, and λ is the control parameter. In our case V_1 contains the "one unit change" matrix elements and V_2 the rest of matrix elements. By varying λ from 0 to 1 in steps 0.1, we study the phase transitional patterns in the same three nuclei. The results can be found in Tables IV-VI and Figures 1-3. We have restricted our study to the yrast states, which exhibit well the effects of a phase transition.

The λ-dependence of the low-energy levels presents a minimum at λ around 0.2-0.3 for all nuclei and for almost all values of nuclear spin (for ^{24}Mg, the minimum of the 2_1^+ state is displaced to $\lambda = 0.3$, while for ^{52}Fe the minimum of the 4_1^+ state is displaced to $\lambda = 0.1$). At the same time, the energy ratio $R_{4/2}$ reaches a maximum, which is always close to a deformed value, just after, or at, the minimum in the energies of the yrast states. For example, for ^{24}Mg the maximum of $R_{4/2}$ appears at $\lambda = 0.4$, while for ^{52}Fe the maximum of $R_{4/2}$ and the minimum of the yrast energies coincide. The case of ^{28}Si is distinct from the other two, since its quadrupole moment changes abruptly from negative to positive values and the $R_{4/2}$

ratio has two maxima for different types of deformation. The second maximal $R_{4/2}$ value appears for $\lambda = 0.3$. Another quantity that reflects the effects of the phase transition is the quadrupole moment of the 2^+ state that has a minimum close to the values of λ where other observables have their extremal values.

We note that the ratio $E(J)/J(J+1)$ (effective inverse moment of inertia) is almost independent of J for all nuclei, from $\lambda = 0.0$ up to the value of λ where the energy ratio $R_{4/2}$ has its maximum for each particular nucleus. The reduced transition probabilities are also sensitive to the phase transition, showing a maximum close to the point of minimum energy of the yrast states. The probabilities $B(\mathrm{E2};6_1^+ \rightarrow 4_1^+)$ for ^{28}Si and ^{52}Fe have a maximum for slightly greater values of λ.

The ground state wave function also displays the signs of a quantum phase transition. Fig. 4 shows the amplitudes of this function expanded in terms of single-particle orbitals for protons and neutrons coupled to angular momenta (J_n, J_p) =(0,0), (2,2), (3,3), (4,4), (6,6) as a function of λ. The results for the amplitudes of the couplings (0,0), (2,2) and (4,4) are quite similar for ^{24}Mg and ^{52}Fe. The (0,0) coupled pairs have their minimum amplitudes for small values of λ while the (2,2) coupled pairs are stronger for the same values of λ. Basically, up until the point of the quantum phase transition, the (2,2) coupled pairs are the strongest components of the ground state wave function, a behavior consistent with deformation characteristics. After the critical point, their amplitudes fall down and the amplitudes of the (0,0) coupled pairs rise, becoming eventually the strongest components of the wave function, a typical feature of the vibrational limit. The amplitudes of the (4,4) coupled pairs have their largest values for the smallest λ and then they slowly decrease, taking an almost steady value after the point of the phase transition. The behavior of the amplitudes of ^{28}Si for $\lambda = 0.0$ and 0.1 differs from other nuclei, as the amplitudes have a steady but still coherent behavior with the (2,2) component being stronger than the (0,0) one, but with a clear predominance of the (3,3) component over all others. This steady behavior suddenly breaks for $\lambda = 0.2$, with the components moving abruptly to the values they would have if the quadrupole moments had had a steady sign following the behavior of the amplitudes in other nuclei. For ^{52}Fe, up to the transitional point, the (6,6) component seems to be also of some importance.

These results suggest that a nuclear system governed by the Hamiltonian (3) undergoes a phase transition at $\lambda = 0.2$, with the rotational characteristics being more evident for $\lambda \leq 0.2$

and declining for $\lambda > 0.2$. One might expect that close to the transition point, where the excitation energies have their minimum values, an enhancement of the level density would be observed, at least at relatively low energy. Previous studies in the framework of the IBM model for large boson numbers have confirmed this enhancement [24] in the spectrum of 0^+ states. Enhancement in the number of low-lying 0^+ states has also been observed experimentally [25] in the rare earth region for the transitional nucleus ^{154}Gd.

In order to search for signs of the collective enhancement, we calculate the number of 0^+ states up to 10 MeV for selected three nuclei at different values of the parameter λ, as shown in Table VII and Figure 5. These results are qualitatively independent of the angular momentum used − different spins show the same behavior of the level density. The number of levels was calculated using the moments method as well as its renormalized version when all level densities are centered at unity.

No signs of collective enhancement are observed just at the transitional point. In all cases there is a sharp drop at the number of levels as a function of λ. This result doesn't change even if we use a smaller energy interval to calculate the number of levels, for instance up to 3 MeV. For ^{28}Si, a peak appears for $\lambda = 0.2$, i.e. at the point of the transition, however this peak has to be attributed to the sudden change of the quadrupole moment at $\lambda = 0.2$, since there is no similar effect in other two nuclei, whose quadrupole moment has a steady sign. The vicinity of the phase transition point that in a finite system is always smeared as a crossover can be studied in more detail by means of the invariant correlational entropy [26].

Last, among the different level densities calculated, we selected those few ones that indicate a spherical or a deformed shape, according to their $R_{4/2}$ value. According to Table VIII where we collected the results, deformed cases always have enhanced level density compared to the spherical cases. This seems to be a general result consistently observed among all the cases studied.

VI. DISCUSSION

In this study, the fixed Hilbert space of the shell model has been probed by varying the numerical parameters of the Hamiltonian while keeping intact all exact conservation laws. This allows us to study the evolution of physical observables and the corresponding level

density. Technically the shell-model Hamiltonian was divided in two parts. The part V_1 included the two-body matrix elements which induce the transfer of one nucleon between the partitions, whereas the part V_2 contained remaining matrix elements. By varying the strength of the two parts of the Hamiltonian, we have followed the changes of the energy spectrum, quadrupole moments and transition probabilities for selected nuclei in the *sd* and *pf* shells. The results confirm that the "one unit change" matrix elements are responsible for the appearance of rotational characteristics, lowering energy of the 2_1^+ and 4_1^+ levels, inducing the $R_{4/2}$ values typical for a rotor and large reduced transition probabilities between rotational states. On the other hand, the V_2 part of the interaction breaks the rotational characteristics and induces a vibrational behavior.

Collective modes in nuclei strongly influence the level density at the low-energy part of the spectrum, the phenomenologically known effect called the *collective enhancement*. By selecting the rotational and vibrational cases resulting from the variation of the shell model Hamiltonian, one can clearly see that the deformed nuclear spectra are richer in low-lying levels compared to the spherical ones, a clear indication of collective enhancement. The enhancement has to be compensated at higher energy unless we extend our orbital space; for the fixed space, the compensation occurs beyond the borderline of applicability of the used shell-model version.

The role of the "one unit change" matrix elements as the carriers of deformation is so pronounced that one can even see a quantum phase transition between deformed and spherical (often with soft vibrations as predecessors of the shape instability) phases of the system, by simultaneously varying the V_1 and V_2 parts of the Hamiltonian. The phase transition reveals itself in the ground state wave function of the system, the energy spectrum and transition probabilities. No similar phase transition has been observed by dividing the Hamiltonian in other combinations. The phase transition reveals itself by the cooperative dynamical action of many components of the interaction present in the shell-model Hamiltonian.

Our preliminary results have shown that in the case in odd-odd nuclei the "one unit change" matrix elements affect noticeably the whole energy spectrum. For odd-odd nuclei we would expect to see signs of collective enhancement even at the transitional point.

Acknowledgments

The work was supported by the NSF grant PHY-1404442. We are thankful to B.A. Brown and R.A. Sen'kov for numerous discussions; V.Z. acknowledges useful discussions with N. Auerbach during the visit to Tel Aviv supported by the Binational Science Foundation US-Israel.

---

[1] H.A. Bethe, Phys. Rev. **50**, 332 (1936); Rev. Mod. Phys. **9**, 69 (1937).

[2] A. Bohr and B.R. Mottelson, *Nuclear Structure*, Vol. I: Single Particle Motion (World Scientific, 1997).

[3] S. Goriely, S. Hilaire, and A.J. Koning, Phys. Rev. C **78**, 064307 (2008).

[4] S. Hilaire, M. Girod, S. Goriely, and A.J. Koning, Phys. Rev. C **86**, 064317 (2012).

[5] F.S. Chang, J.B. French, and T.H. Thio, Ann. Phys. **66**, 137 (1971).

[6] G. Hansen and A.S. Jensen, Nucl. Phys. **A406**, 236 (1983).

[7] A.V. Ignatyuk, K.K. Istekov, and G.N. Smirenkin, Sov. J. Nucl. Phys. **29**, 450 (1979).

[8] T. Døssing and A. S. Jensen, Nucl. Phys. A **222**, 493 (1974).

[9] S. Bjørnholm, A. Bohr, and B.R. Mottelson, Physics and Chemistry of Fission **1**, 367 (IAEA, Vienna, 1974).

[10] A. Bohr and B.R. Mottelson, *Nuclear Structure*, Vol. II: Nuclear Deformations (World Scientific, 1998).

[11] T. Ericson, Nucl. Phys. **6**, 62 (1958).

[12] V.K.B. Kota and R.U. Haq, eds., *Spectral Distributions in Nuclei and Statistical Spectroscopy* (World Scientific, Singapore, 2010).

[13] S.S.M. Wong, *Nuclear Statistical Spectroscopy* (Oxford University Press, 1986).

[14] R.A. Sen'kov, M. Horoi, and V.G. Zelevinsky, Phys. Lett. B **702**, 413 (2011).

[15] R.A. Sen'kov, M. Horoi, and V.G. Zelevinsky, Computer Physics Communications **184**, 215 (2013).

[16] R.A. Sen'kov and V. Zelevinsky, arXiv:1508.0368.

[17] M. Horoi and V. Zelevinsky, Phys. Rev. C **81**, 034306 (2010).

[18] H. Chen, J.R. Brownstein, and D.J. Rowe, Phys. Rev. C **42**, 1422 (1990).

[19] C. Bahri, D.J. Rowe, and W. Wijesundera, Phys. Rev. C **58**, 1539 (1998).

[20] D.J. Rowe, Nucl. Phys. **A745**, 47 (2004).

[21] Y. A. Luo, F. Pan, T. Wang, P. Z. Ning, and J.P. Draayer, Phys. Rev. C **73**, 044323 (2006).

[22] Y. Luo, Y. Zhang, X. Meng, F. Pan, and J.P. Draayer, Phys. Rev. C **80**, 014311 (2009).

[23] P. Cejnar, J. Jolie, and R. F. Casten, Rev. Mod. Phys. **82**, 2155 (2010).

[24] P. Cejnar and J. Jolie, Phys. Rev. E **61**, 6237 (2000).

[25] D.A. Meyer, V. Wood, R.F. Casten, C.R. Fitzpatrick, G. Graw, D. Bucurescu, J. Jolie, P. von Brentano, R. Hertenberger, H.-F. Wirth, N. Braun, T. Faestermann, S. Heinze, J.L. Jerke, R. Krucken, M. Mahgoub, O. Moller, D. Mucher, and C. Scholl, Phys. Rev. C **74**, 044309 (2006).

[26] A. Volya and V. Zelevinsky, Phys. Lett. B **574**, 27 (2003).

Figures

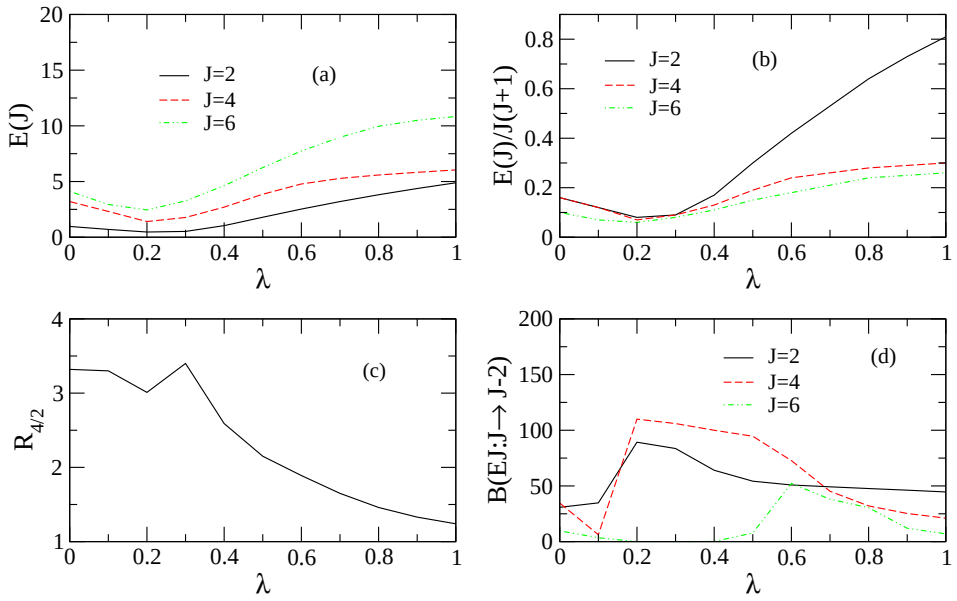

FIG. 1: (a) Yrast 2^+, 4^+, 6^+ energies, (b) ratios $E(J)/J(J+1)$ for $J = 0, 2, 4$, (c) ratios $R_{4/2}$, (d) electromagnetic transition rates between them as a function of λ for ^{28}Si.

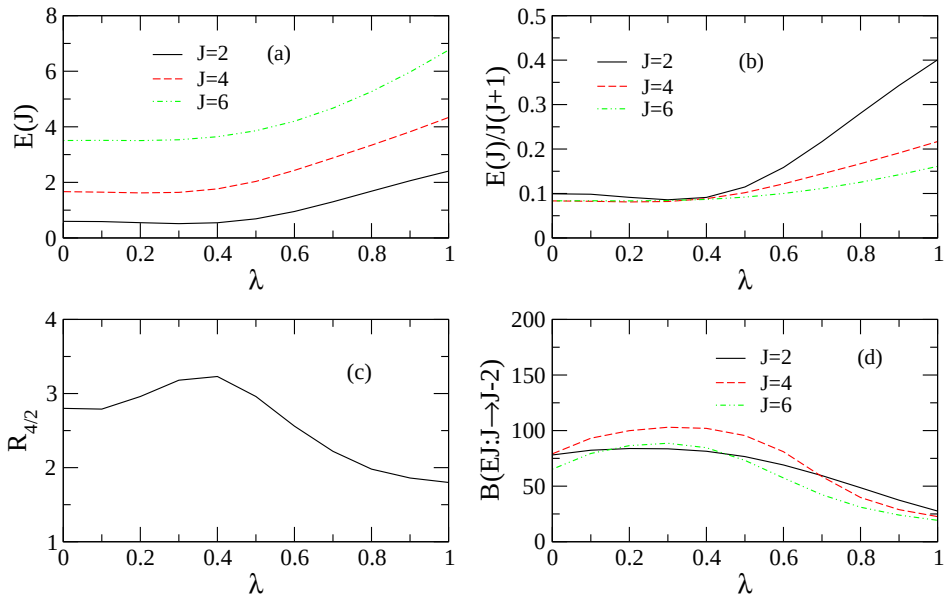

FIG. 2: (a) Yrast 2^+, 4^+, 6^+ energies, (b) ratios $E(J)/J(J+1)$ for $J = 0, 2, 4$, (c) ratios $R_{4/2}$, (d) electromagnetic transition rates between them as a function of λ for ^{24}Mg.

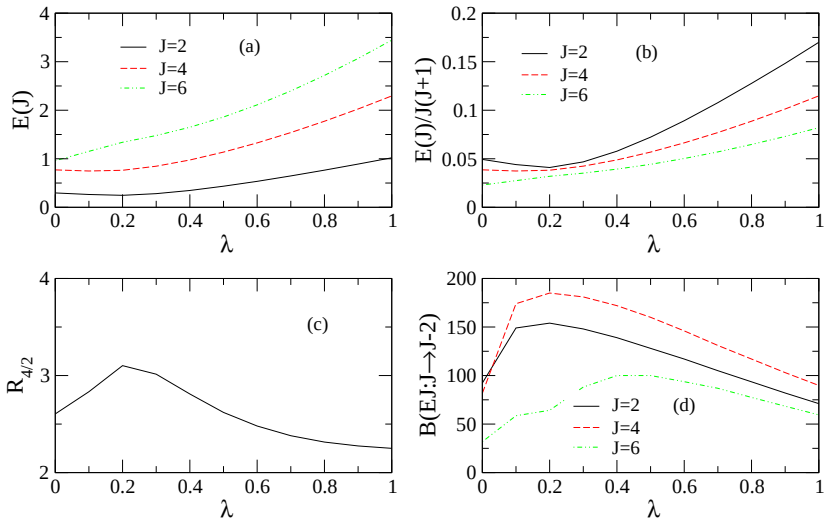

FIG. 3: (a) Yrast 2^+, 4^+, 6^+ energies, (b) ratios $E(J)/J(J+1)$ for $J = 0, 2, 4$, (c) ratios $R_{4/2}$, (d) electromagnetic transition rates between them as a function of λ for ^{52}Fe.

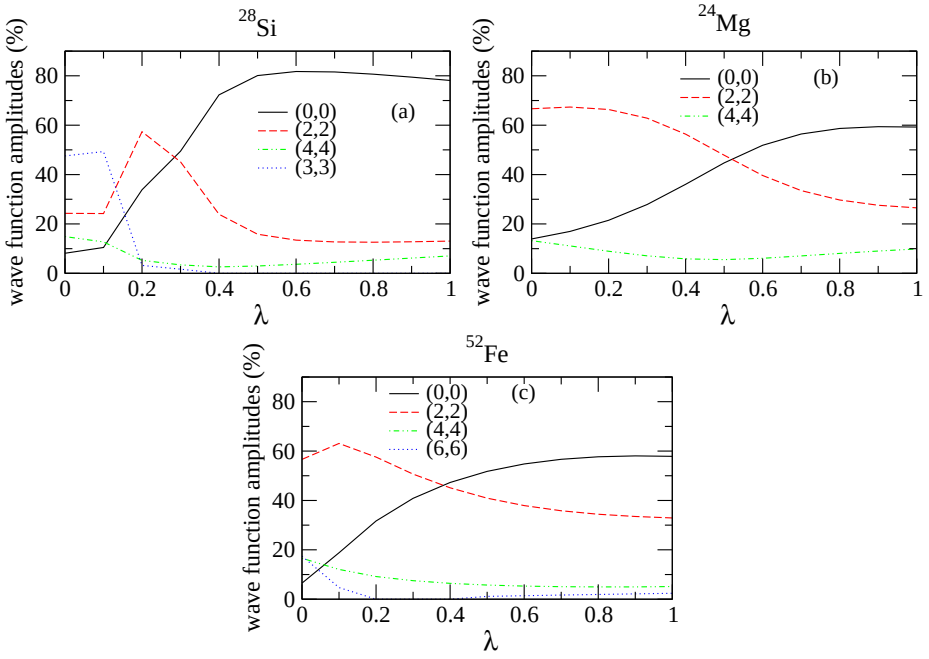

FIG. 4: Amplitudes of the ground state wave function expanded in terms of the proton and neutron components coupled to angular momenta (0,0), (2,2), (3,3), (4,4), (6,6) as a function of λ for (a) ^{28}Si, (b) ^{24}Mg, and (c) ^{52}Fe.

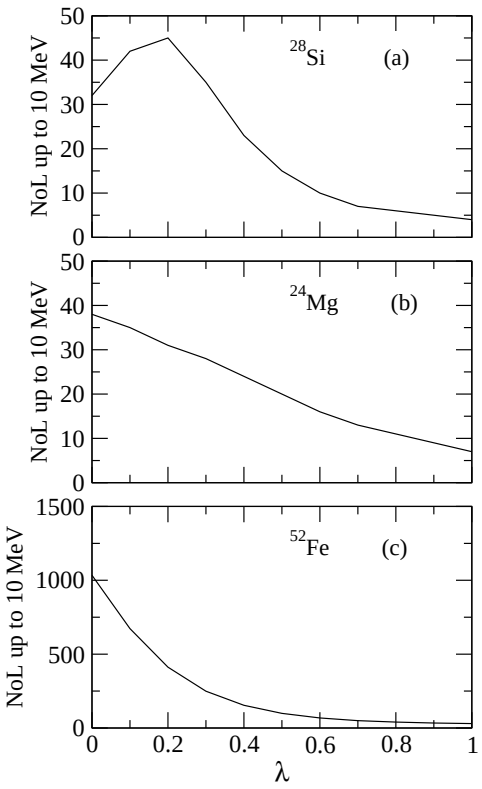

FIG. 5: Number of levels up to 10 MeV as a function of λ for (a) ^{28}Si, (b) ^{24}Mg, (c) ^{52}Fe.

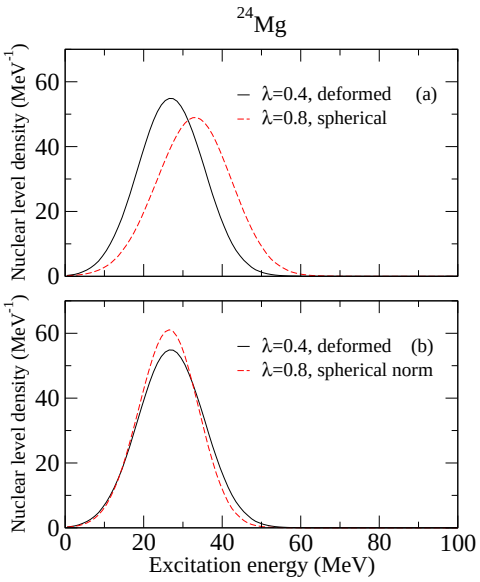

FIG. 6: Nuclear level densities for $J = 0$, for ^{24}Mg and for the points given in Table VIII. The upper panel, (a), corresponds to the level density as given by the moments method. The lower panel, (b), shows the level density that corresponds to the spherical case, normalised to the width of the deformed level density.

Tables

TABLE I: Results for k_1=1.0 and changing k_2 for yrast energies (MeV) of 2^+ and 4^+ levels, ratios $R_{4/2}$, quadrupole moments $Q(2_1^+)$ (e·fm^2) and reduced transition probabilities $B(\mathrm{E2};2_1^+ \to 0_1^+)$ (e$^2 \cdot$ fm^4) for ^{28}Si, ^{24}Mg, and ^{52}Fe.

^{28}Si, k_1=1.0					
k_2	$E(2_1^+)$	$E(4_1^+)$	$R_{4/2}$	$Q(2_1^+)$	$B(\mathrm{E2};2_1^+ \to 0_1^+)$
0.0	0.964	3.197	3.32	-11.50	30.75
0.1	0.866	2.797	3.23	-12.21	35.54
0.2	0.775	1.881	2.42	20.12	9.75
0.3	0.628	1.966	3.13	21.06	109.4
0.4	0.685	2.266	3.31	21.46	112.7
0.5	0.781	2.603	3.33	21.62	113.9
0.6	0.925	2.975	3.21	21.61	113.0
0.7	1.122	3.377	3.01	21.52	110.5
0.8	1.369	3.801	2.78	21.33	107.2
0.9	1.659	4.233	2.55	21.27	103.6
1.0	1.987	4.658	2.34	18.79	81.93
^{24}Mg, k_1=1.0					
k_2	$E(2_1^+)$	$E(4_1^+)$	$R_{4/2}$	$Q(2_1^+)$	$B(\mathrm{E2};2_1^+ \to 0_1^+)$
0.0	0.596	1.667	2.80	-16.32	78.09
0.1	0.636	1.795	2.82	-18.04	83.40
0.2	0.661	1.931	2.92	-18.80	86.61
0.3	0.689	2.095	3.04	-19.28	89.04
0.4	0.731	2.297	3.14	-19.59	90.99
0.5	0.794	2.541	3.20	-19.77	92.54
0.6	0.882	2.828	3.21	-19.84	93.83
0.7	0.998	3.158	3.16	-19.81	94.87
0.8	1.142	3.529	3.09	-19.70	95.75
0.9	1.313	3.937	3.00	-19.51	96.27
1.0	1.509	4.378	2.90	-17.44	79.12

^{52}Fe, k_1=1.0					
k_2	$E(2_1^+)$	$E(4_1^+)$	$R_{4/2}$	$Q(2_1^+)$	$B(\mathrm{E2};2_1^+ \rightarrow 0_1^+)$
0.0	0.296	0.771	2.60	-20.68	92.28
0.1	0.312	0.854	2.74	-25.76	152.60
0.2	0.319	0.951	2.98	-27.16	168.80
0.3	0.353	1.081	3.06	-27.92	176.70
0.4	0.401	1.232	3.07	-28.48	182.40
0.5	0.461	1.397	3.03	-28.92	187.50
0.6	0.528	1.576	2.98	-29.32	192.60
0.7	0.604	1.768	2.93	-29.70	198.20
0.8	0.688	1.975	2.87	-30.07	204.70
0.9	0.781	2.197	2.81	-30.42	212.20
1.0	0.883	2.434	2.76	-30.76	221.10

TABLE II: Results for k_1=1.0 and changing k_2 for yrast energies (MeV) of 2^+ and 4^+ levels, ratios $R_{4/2}$, quadrupole moments $Q(2_1^+)$ ($\mathrm{e}\cdot\mathrm{fm}^2$) and reduced transition probabilities $B(\mathrm{E2};2_1^+ \to 0_1^+)$ ($\mathrm{e}^2\cdot\mathrm{fm}^4$) for ^{28}Si, ^{24}Mg, and ^{52}Fe.

^{28}Si, k_2=1.0					
k_1	$E(2_1^+)$	$E(4_1^+)$	$R_{4/2}$	$Q(2_1^+)$	$B(\mathrm{E2};2_1^+ \to 0_1^+)$
0.0	4.886	6.039	1.24	4.52	44.58
0.1	4.798	6.019	1.25	6.07	48.05
0.2	4.654	5.979	1.28	7.79	51.52
0.3	4.452	5.918	1.33	9.66	55.05
0.4	4.192	5.833	1.39	11.60	58.69
0.5	3.875	5.721	1.47	13.52	62.73
0.6	3.510	5.576	1.59	15.35	67.49
0.7	3.112	5.392	1.73	17.02	73.42
0.8	2.705	5.165	1.91	18.49	80.88
0.9	2.320	4.909	2.12	19.74	90.06
1.0	1.987	4.658	2.34	18.79	81.93
^{24}Mg, k_2=1.0					
k_1	$E(2_1^+)$	$E(4_1^+)$	$R_{4/2}$	$Q(2_1^+)$	$B(\mathrm{E2};2_1^+ \to 0_1^+)$
0.0	2.404	4.337	1.80	-7.29	27.61
0.1	2.380	4.372	1.84	-9.56	37.65
0.2	2.308	4.421	1.92	-11.81	48.48
0.3	2.198	4.472	2.03	-13.76	58.82
0.4	2.067	4.504	2.18	-15.32	67.86
0.5	1.932	4.499	2.33	-16.51	75.50
0.6	1.808	4.465	2.47	-17.40	81.77
0.7	1.702	4.423	2.60	-18.08	86.86
0.8	1.618	4.391	2.71	-18.58	90.91
0.9	1.554	4.375	2.82	-18.97	94.09
1.0	1.509	4.378	2.90	-17.44	79.12

^{52}Fe, k_2=1.0					
k_1	$E(2_1^+)$	$E(4_1^+)$	$R_{4/2}$	$Q(2_1^+)$	$B(\mathrm{E2};2_1^+ \to 0_1^+)$
0.0	1.020	2.295	2.25	-14.79	71.06
0.1	1.020	2.299	2.25	-16.42	82.66
0.2	1.015	2.306	2.27	-18.08	94.96
0.3	1.006	2.316	2.30	-19.75	107.90
0.4	0.993	2.327	2.34	-21.40	121.40
0.5	0.978	2.342	2.39	-23.02	135.40
0.6	0.960	2.359	2.46	-24.59	149.80
0.7	0.941	2.378	2.53	-26.13	165.10
0.8	0.923	2.399	2.60	-27.65	181.30
0.9	0.903	2.420	2.68	-29.18	199.60
1.0	0.883	2.434	2.76	-30.76	221.10

TABLE III: Cumulative Number of Levels (NoL) of $J = 0$ up to energy 10 MeV for different (k_1, k_2) combinations for ^{28}Si, ^{24}Mg and ^{52}Fe found with the moments method. The column NoL corresponds to the calculation of the moments method, while the column Renorm corresponds to the renormalized level density (NoL up to 0.4).

shape	case	nucleus	$R_{4/2}$	NoL	Renorm
deformed	$k_1 = 1.0, k_2 = 0.4$	^{28}Si	3.31	22	60
deformed	$k_1 = 1.0, k_2 = 0.5$	^{28}Si	3.33	17	54
deformed	$k_1 = 1.0, k_2 = 0.6$	^{28}Si	3.21	13	49
spherical	$k_2 = 1.0, k_1 = 0.9$	^{28}Si	2.12	5	34
deformed	$k_1 = 1.0, k_2 = 0.5$	^{24}Mg	3.20	10	24
deformed	$k_1 = 1.0, k_2 = 0.6$	^{24}Mg	3.21	8	21
spherical	$k_2 = 1.0, k_1 = 0.3$	^{24}Mg	2.03	6	18
deformed	$k_1 = 1.0, k_2 = 0.4$	^{52}Fe	3.07	236	6516
spherical	$k_2 = 1.0, k_1 = 0.0$	^{52}Fe	2.25	30	2617

TABLE IV: Yrast energies of 2^+, 4^+ and 6^+ (MeV), ratios $R_{4/2}$, quadrupole moments $Q(2_1^+)$ ($e \cdot fm^2$) and reduced transition probabilities $B(E2;2_1^+ \to 0_1^+)$, $B(E2;4_1^+ \to 2_1^+)$, $B(E2;6_1^+ \to 4_1^+)$ ($e^2 \cdot fm^2$) for ^{28}Si

λ	2_1^+	4_1^+	6_1^+	$R_{4/2}$	$Q(2_1^+)$	B(E2;$2_1^+ \to 0_1^+$)	B(E2;$4_1^+ \to 2_1^+$)	B(E2;$6_1^+ \to 4_1^+$)
0.0	0.964	3.197	4.110	3.32	-11.5	30.75	34.61	9.70
0.1	0.702	2.314	2.938	3.30	-12.14	34.80	6.22	3.46
0.2	0.469	1.410	2.447	3.01	18.74	89.30	109.60	0.10
0.3	0.521	1.771	3.257	3.40	18.63	83.56	105.80	0.06
0.4	1.041	2.699	4.624	2.59	17.36	64.08	100.40	0.16
0.5	1.793	3.857	6.252	2.15	15.42	54.32	94.61	7.77
0.6	2.529	4.777	7.739	1.89	13.1	50.94	72.65	52.32
0.7	3.203	5.280	8.973	1.65	10.7	49.24	45.16	38.08
0.8	3.815	5.587	9.959	1.46	8.41	47.74	32.07	30.52
0.9	4.373	5.826	10.492	1.33	6.35	46.21	25.30	11.96
1.0	4.886	6.039	10.842	1.24	4.52	44.58	21.07	6.97

TABLE V: Yrast energies of 2^+, 4^+ and 6^+ (MeV), ratios $R_{4/2}$, quadrupole moments $Q(2_1^+)$ (e·fm^2) and reduced transition probabilities $B(\mathrm{E2};2_1^+ \to 0_1^+)$, $B(\mathrm{E2};4_1^+ \to 2_1^+)$, $B(\mathrm{E2};6_1^+ \to 4_1^+)$ (e$^2 \cdot$ fm^2) for ^{24}Mg

λ	2_1^+	4_1^+	6_1^+	$R_{4/2}$	$Q(2_1^+)$	B(E2;$2_1^+ \to 0_1^+$)	B(E2;$4_1^+ \to 2_1^+$)	B(E2;$6_1^+ \to 4_1^+$)
0.0	0.596	1.667	3.507	2.80	-16.32	78.09	79.09	65.32
0.1	0.590	1.649	3.512	2.79	-18.02	82.34	93.06	79.36
0.2	0.548	1.620	3.504	2.96	-18.65	83.89	99.93	86.48
0.3	0.515	1.640	3.533	3.18	-18.87	83.64	102.70	88.61
0.4	0.547	1.766	3.642	3.23	-18.68	81.37	101.50	84.58
0.5	0.688	2.036	3.860	2.96	-17.97	76.60	95.45	73.21
0.6	0.951	2.433	4.201	2.56	-16.65	69.12	81.00	57.41
0.7	1.300	2.881	4.672	2.22	-14.71	59.51	58.57	42.26
0.8	1.683	3.339	5.267	1.98	-12.28	48.55	39.82	31.08
0.9	2.058	3.821	5.970	1.86	-9.68	37.37	28.94	23.99
1.0	2.404	4.337	6.761	1.80	-7.29	27.61	22.63	19.30

TABLE VI: Yrast energies of 2^+, 4^+ and 6^+ (MeV) states, ratios $R_{4/2}$, quadrupole moments $Q(2_1^+)$ ($e \cdot fm^2$) and reduced transition probabilities $B(E2;2_1^+ \to 0_1^+)$, $B(E2;4_1^+ \to 2_1^+)$, $B(E2;6_1^+ \to 4_1^+)$ ($e^2 \cdot fm^2$) for ^{52}Fe

λ	2_1^+	4_1^+	6_1^+	$R_{4/2}$	$Q(2_1^+)$	B(E2;$2_1^+ \to 0_1^+$)	B(E2;$4_1^+ \to 2_1^+$)	B(E2;$6_1^+ \to 4_1^+$)
0.0	0.296	0.771	0.960	2.61	-20.68	92.28	81.66	31.76
0.1	0.264	0.748	1.154	2.83	-25.27	149.20	173.90	58.55
0.2	0.246	0.763	1.340	3.10	-25.60	154.10	184.90	64.16
0.3	0.281	0.847	1.479	3.01	-25.02	148.00	181.30	88.09
0.4	0.347	0.975	1.649	2.81	-24.00	138.50	171.80	100.30
0.5	0.434	1.137	1.860	2.62	-22.70	127.90	159.50	100.10
0.6	0.535	1.327	2.111	2.48	-21.24	116.60	145.80	93.69
0.7	0.647	1.540	2.397	2.38	-19.68	105.10	131.40	86.89
0.8	0.766	1.773	2.717	2.32	-18.06	93.48	117.10	77.49
0.9	0.890	2.025	3.067	2.28	-16.42	82.01	103.20	68.40
1.0	1.020	2.295	3.444	2.25	-14.79	71.06	89.81	59.53

TABLE VII: Cumulative Number of Levels (NoL) with $J = 0$ up to energy 10 MeV for different values of λ for ^{28}Si, ^{24}Mg and ^{52}Fe. The column NoL corresponds to the calculation of the moments method, while the column Renorm corresponds to the renormalized level density (NoL up to 0.4 MeV).

^{28}Si			^{24}Mg			^{52}Fe		
λ	NoL	Renorm	λ	NoL	Renorm	λ	NoL	Renorm
0.0	32	67	0.0	38	44	0.0	1034	12853
0.1	42	75	0.1	35	40	0.1	673	10435
0.2	45	75	0.2	31	36	0.2	412	8278
0.3	35	63	0.3	28	33	0.3	249	6581
0.4	23	49	0.4	24	31	0.4	154	5284
0.5	15	38	0.5	20	28	0.5	99	4354
0.6	10	31	0.6	16	26	0.6	68	3746
0.7	7	27	0.7	13	24	0.7	50	3248
0.8	6	24	0.8	11	22	0.8	40	2942
0.9	5	23	0.9	9	20	0.9	34	2731
1.0	4	22	1.0	7	19	1.0	30	2617

TABLE VIII: Cumulative Number of Levels (NoL) up to 10 MeV energy for spherical or deformed cases which appear for various values of λ for ^{28}Si, ^{24}Mg, and ^{52}Fe nuclei

shape	case	nucleus	$R_{4/2}$	NoL
deformed	λ=0.0	^{28}Si	3.32	32
spherical	λ=0.5	^{28}Si	2.15	15
deformed	λ=0.4	^{24}Mg	3.23	24
spherical	λ=0.8	^{24}Mg	1.98	11
deformed	λ=0.2	^{52}Fe	3.10	412
spherical	λ=1.0	^{52}Fe	2.25	30